HHS Public Access

Author manuscript

Nanomedicine (Lond). Author manuscript; available in PMC 2016 March 01.

Published in final edited form as:

Nanomedicine (Lond). 2015 May ; 10(10): 1555–1568. doi:10.2217/nnm.15.14.

Metabolic and structural integrity of magnetic nanoparticle-loaded primary endothelial cells for targeted cell therapy

Zulfiya Orynbayeva[*,1], **Richard Sensenig**[2], and **Boris Polyak**[**,1,3]

[1]Department of Surgery, Drexel University College of Medicine, Philadelphia, PA 19102, USA

[2]Department of Surgery, University of Pennsylvania, Philadelphia, PA 19104, USA

[3]Department of Pharmacology & Physiology, Drexel University College of Medicine, Philadelphia, PA 19102, USA

Abstract

Aim—To successfully translate magnetically mediated cell targeting from bench to bedside, there is a need to systematically assess the potential adverse effects of magnetic nanoparticles (MNPs) interacting with 'therapeutic' cells. Here, we examined in detail the effects of internalized polymeric MNPs on primary rat endothelial cells' structural intactness, metabolic integrity and proliferation potential.

Materials & methods—The intactness of cytoskeleton and organelles was studied by fluorescent confocal microscopy, flow cytometry and high-resolution respirometry.

Results—MNP-loaded primary endothelial cells preserve intact cytoskeleton and organelles, maintain normal rate of proliferation, calcium signaling and mitochondria energy metabolism.

Conclusion—This study provides supportive evidence that MNPs at doses necessary for targeting did not induce significant adverse effects on structural integrity and functionality of primary endothelial cells – potential cell therapy vectors.

Keywords

Ca^{2+} signaling; cytoskeleton; magnetic nanoparticles; mitochondria membrane potential; mitochondria oxidative phosphorylation; primary endothelial cells

[*]Author for correspondence: Tel.: +1 215 762 2052, Fax: +1 215 762 8389, zorynbay@drexelmed.edu. [**]Author for correspondence: Tel.: +1 215 762 3386, Fax: +1 215 762 8389, bpolyak@drexelmed.edu.

Disclaimer

The content is solely the responsibility of the authors and does not necessarily represent the official views of the National Heart, Lung and Blood Institute or the National Institutes of Health.

Ethical conduct of research

The authors state that they have obtained appropriate institutional review board approval or have followed the principles outlined in the Declaration of Helsinki for all human or animal experimental investigations. In addition, for investigations involving human subjects, informed consent has been obtained from the participants involved.

Financial & competing interests disclosure

This study was funded by the National Heart, Lung and Blood Institute (award number R01HL107771). The authors have no other relevant affiliations or financial involvement with any organization or entity with a financial interest in or financial conflict with the subject matter or materials discussed in the manuscript apart from those disclosed.

No writing assistance was utilized in production of this manuscript.

Cell-based therapy is one of the promising and rapidly growing fields of translational medicine. Initially, cell-based therapeutics was used for blood transfusions and bone marrow transplantations. However, recent advances in cell and molecular biology have expanded the potential applications of this approach. Cells are currently used as substitutes for diseased or damaged cells and tissues (cell replacement therapy), components in reconstruction of regenerated tissues (tissue engineering), as well as drug delivery vehicles.

In order to realize the great potential of cell-based therapy, a number of formidable tasks still has to be addressed. These include achieving immune tolerance (if nonautologous cells are used), developing biomimetic materials for tissue engineering, controlling stem cell differentiation and developing the means of efficient localization of cell-based therapy. One way to target a diseased tissue and specifically localize therapeutic cells is by generation of magnetic force. In this approach, the delivered cells have to be loaded with magnetic particles to be responsive to a magnetic force generated by an applied magnetic field gradient. Magnetic particles develop magnetic polarization and magnetophoretic mobility when an external magnetic field and field gradient are applied [1]. Therefore, by means of selective application of a magnetic field gradient to a desired area, cells bearing magnetic particles can be successfully targeted to the desired anatomical site with a relatively high accuracy, minimum surgical intervention and maximum effective dose. In this way, the efficacy of regional cell therapy could be improved by increasing local accumulation of therapeutic cells, while systemic distribution of ‘therapy’ and undesired side effects may be significantly decreased or eliminated [2].

Our group is currently investigating a therapeutic strategy based on magnetic targeting of endothelial cells to intravascular stents [3] to prevent repeatable blockages of stented arteries, in other words, in-stent restenosis due to growth of newly resided smooth muscle cells. Studies have shown that accelerated re-endothelialization following arterial injury inhibits smooth muscle cell migration and proliferation [4] and therefore has the potential to prevent or reduce intimal hyperplasia [5]. Early restoration of endothelial integrity has been shown to modify thrombogenic and proliferative vascular wall properties in a number of animal models [6–10]. Clinical observations and animal studies have led investigators to test the hypothesis that enhancing re-endothelialization might inhibit neointimal formation following vascular injury. Indeed, early restoration of endothelial integrity through local VEGF administration was associated with reduced proliferation of intimal vascular smooth muscle cells, providing indirect evidence to support a role of endothelial integrity in suppressing intimal hyperplasia [11–13].

While developing a future clinical implementation for such magnetic cell therapy approach, it is very crucial to obtain comprehensive information about cell structural and metabolic stability to ensure future therapeutic efficacy along with minimal or no adverse effects caused by introduction of nanomagnetic materials to the delivered cells and to the patient. The functionality of major cell organelles guarantees metabolic stability of the central energy supplying system, the cell trafficking machinery, the signaling and proliferative apparatus of the cell and ensures proper cell activity and lifespan necessary for achieving a desired therapeutic effect. In this work we examined in detail the effects of internalized

polymeric magnetic nanoparticles (MNPs) on cell structural and metabolic integrity and cell potential for further proliferation. Intactness of cytoskeleton elements and major organelles, such as endoplasmic reticulum (ER) and mitochondria, involved in cellular calcium and energy homeostasis, were investigated to validate magnetically loaded cells functional competence and stability.

Materials & methods

Cell culture & loading with magnetic nanoparticles

Primary rat aortic endothelial cells (RAECs) were isolated and characterized as described elsewhere [14]. These cells represent a highly pure culture of endothelial cells (98% CD31 and 90% Tie-2 positive, and 4% α-SMA negative by flow cytometry [14]).

Polylactic acid (PLA)-based magnetite-loaded nanoparticles (MNPs) were prepared by the modified emulsification-solvent evaporation method as previously described [15,16]. The particles contained 48.2 ± 1.32% (w/w) magnetite (per spectrophotometry) and were fluorescently labeled by BODIPY®564/570 nm (Life Technologies, NY, USA) as described elsewhere [17]. Briefly, poly(DL-lactide) with the carboxylic end terminated with dodecyl groups (HO-PLA-$OC_{12}H_{25}$) was acylated with N-(tert-butoxycarbonyl)glycine (Boc-Gly-OH) in dichloromethane by using 1-ethyl-3-(3-dimethylaminopropyl) carbodiimide hydrochloride as an activator and N,N-dimethylaminopyridine tosylate as a catalyst. After removal of the Boc-protection, the resulting amino-functionalized polymer was reacted with BODIPY®564/570 N-succinimidyl esters [17]. The MNPs had a mean hydrodynamic diameter of 278 ± 1.62 nm and ζ-potential of −14.4 ± 0.34 mV. Magnetization of the MNPs measured at 5 kOe was 24.6 ± 1.22 emu/g of MNP composite. Full characterization of MNPs can be found in [18].

For cell loading, RAECs were seeded on clear-bottom six-well plates (BD Biosciences, CA, USA) using Endothelial Basal Medium MCDB 131 medium (Mediatech Inc., VA, USA) supplemented with 5% fetal bovine serum, EGF (10 ng/ml), hydrocortisone (1 μg/ml) and L-glutamine (10 mM). Twenty microliters (an equivalent of 0.736 mg MNP dry weight) of the original MNP suspension were dispersed in 10 ml of the cell culture medium and filtered through a Millipore syringe driven filter with 5.0 μm pores (Millipore Inc., MA, USA). 1 ml of the diluted MNP suspension (0.0736 mg MNP dry weight) was given to 300,000–350,000 cells and incubated at 37°C for 24 h on a 96-well magnetic separator with an average surface field of 500 Gauss and field gradient of 32.5 T/m as a magnetic field and field gradient source (LifeSep 96F, Dexter Magnetic Technologies, IL, USA). After 24 h, the magnetite content within RAECs was found to be 25.3 ± 0.75 pg magnetite/cell as quantified by the method described elsewhere [19,20]. Briefly, after loading with MNPs the cells were rinsed three-times with PBS, trypsinized and counted. Then, cell suspensions were centrifuged, and the remaining pellet was digested with radioimmunoprecipitation assay cell lysis (RIPA) buffer (Thermo Fisher Scientific, MA, USA). After the centrifugation step, the iron content was determined spectrophotometrically using Synergy™ 4 plate reader (BioTek Instruments Inc., VT, USA) and ultraviolet (UV) compatible 96-well plates, BD Biosciences in 1N hydrochloric acid (λ= 335 nm) against a standard curve after MNP degradation with 1N

aqueous sodium hydroxide (90°C, 30 min) and dissolution of the iron containing precipitate in the acid solution.

Visualization of intracellular organelles

For microscopy experiments, cells were seeded on collagen precoated 35 mm MatTek glass bottom dishes (MatTek Corp., MA, USA) at a density of 300,000 cells per dish. For experiments lasting for few days, cells were seeded at 1.5–3-times lower density. To visualize actin filaments, RAECs were transfected with enhanced yellow fluorescent protein (EYFP)-β-actin plasmid (provided by Dr. G. Gallo, Temple University, PA, USA) using GenDrill DNA *in vitro* transfection reagent according to the manufacturer's protocol (BamaGen BioScience, MD, USA). The same Gen-Drill transfection agent was used to introduce green fluorescent protein (GFP)-tubulin plasmid to visualize microtubules. Cells expressing fluorescent EYFP-β-actin or GFP-tubulin were loaded overnight with BODIPY®564/570 nm MNPs 24 h post-transfection. Before microscopy imaging, cells were rinsed vigorously with Ca^{2+} and Mg^{2+} containing PBS to wash out MNPs not taken up by cells and kept in a modified Krebs buffer: 137 mM NaCl, 5 mM KCl, 1 mM KH_2PO_4, HEPES 20 mM, pH 7.4, 1 mM $MgCl_2$, 2mM $CaCl_2$, 10 mM glucose.

To visualize endoplasmic reticulum (ER), cells were first loaded overnight with BODIPY®564/570 MNPs. The next day noninternalized nanoparticles were removed by several intensive washings with Ca^{2+} and Mg^{2+} containing PBS prior to labeling with 200 nM ER-Tracker Blue-White DPX (Ex/Em wavelengths 374/430 nm; Life Technologies, NY, USA). After 15-min incubation at room temperature in the dark, cells were rinsed and left in the last wash in a modified Krebs buffer described above for imaging.

To visualize mitochondria, both unloaded and loaded with nanoparticles, cells were stained with 24 nM MitoTracker Orange CM™Ros (Ex/Em wavelengths 554/576 nm) and/or with 70 nM MitoTracker Green FM (Ex/Em wavelengths 490/516 nm; Life Technologies). After 15-min incubation at room temperature in the dark, cells were rinsed and left in the last wash for imaging.

To demonstrate the proliferative state, cells were labeled with 14 μg/ml acridine orange (Ex/Em wavelengths 500/526 nm; Life Technologies), a membrane-permeable nucleic acid binding dye, immediately before imaging.

The microscopy studies were performed using Olympus FluoView FV1000 confocal laser scanning inverted microscope (Olympus America. Inc., PA, USA), which enables parallel video imaging and micro-fluorimetry for monitoring modulations in intracellular calcium concentration and mitochondria membrane potential caused by cell loading with nanoparticles. Differential interference contrast (DIC) option enables 3D imaging of cells.

Microscopy measurements of cellular free calcium

RAECs seeded on MatTek glass-bottom dishes at full confluence were loaded with 2 μM Fluo-4AM free calcium-sensitive dye (Ex/Em wavelengths 488/560 nm) in a modified Krebs buffer (see above). After 15-min incubation at 25°C in the dark, cells were washed twice and kept in the buffer for an additional 15 min for stabilization. Cell examination

revealed uniform distribution of Fluo-4AM throughout the cells, suggesting no compartmentalization of Fluo-4AM within the organelles. The average fluorescence intensity of Fluo-4AM measured over each tested cell was converted to Ca^{2+} concentration using the equation [21]:

$$[Ca^{2+}]_c = K_d(F - F_{min})/(F_{max} - F)$$

where F_{min} and F_{max} are the Fluo-4 fluorescence intensity for Ca^{2+}-lacking and Ca^{2+}-saturation concentrations determined by permeabilization of the cells with 10 μM Ionomycin in the presence of 20 mM ethylene glycol tetraacetic acid (EGTA) and 2 mM $CaCl_2$, respectively. Dissociation constant (K_d) for the Fluo-4/Ca complex has been taken as 345 nM according to the manufacturer.

To evaluate the amount of calcium released exclusively from ER, cells were kept in calcium-free buffer described above to exclude extracellular calcium influx. Just prior to examination, RAECs were additionally exposed to 2 μg/ml oligomycin to block the mitochondria adenosine triphosphate synthase in order to avoid energy-dependent calcium sequestration through mitochondria Ca^{2+}-uniporter. On the final step of cell permeabilization with Ionomycin, calcium-free extracellular buffer was replaced with the buffer containing 2 mM $CaCl_2$ followed by chelating Ca^{2+} with 20 mM EGTA.

Evaluation of mitochondria mass & mitochondria membrane potential

RAECs were loaded with nonfluorescent nanoparticles for 24 h prior to measurements. The loaded cells were washed out several times to remove noninternalized MNPs. Then cells were trypsinized and re-suspended in modified Krebs buffer for labeling with fluorescent dyes. MitoTracker Green FM (70 nM; Ex/Em wavelengths 490/516 nm; Life Technologies) fluorescence has been used to designate mitochondria. Cells were observed using 60× NA 1.42 PLAPON oil objective.

Mitochondria membrane potential was examined on BD Accuri C6 flow cytometer (BD Biosciences) by the cells' double labeling with 70nM MitoTracker Green FM and 24 nM MitoTracker Orange CM™Ros (Ex/Em wavelengths 554/576 nm; Life Technologies), the fluorescence of which were used as a measure of mitochondrial mass and mitochondria inner membrane potential, correspondingly. Treatment of the cells with 1 μM of carbonyl cyanide 4-(trifluoromethoxy)phenylhydrazone (FCCP), which uncouples mitochondria oxidative phosphorylation resulting in a collapse of membrane potential, was used as a positive control for mitochondria membrane depolarization.

High-resolution respirometry

The activity of the respiratory system enzymes was analyzed by high-resolution respirometry at 37°C in a two chamber respirometer OROBOROS Oxygraph-2K (Oroboros, Innsbruck, Austria) [22–24]. The OROBOROS DatLab software was used for data acquisition and analysis. Briefly, MNP-loaded and unloaded cells were harvested by centrifugation, rinsed with and resuspended in a modified Krebs buffer as described above. To assess the endogenous energy capacity of cells, no respiratory substrates (glucose or

pyruvate) were added to the measurement chambers. To assess the functional integrity of adenosine triphosphate synthase, 2 μg/ml oligomycin was applied to inhibit the enzyme. Next, to determine the maximum capacity of the mitochondria electron transport system, cells were sequentially titrated with 20 nM dose of FCCP. Respiratory rates were expressed per million of cells, per second. At the end of the measurement, 2.5 μM antimycin was added to evaluate residual oxygen consumption unrelated to mitochondria respiration.

Analysis of apoptosis/necrosis

About 10^6 cells loaded and unloaded with MNPs were harvested and double stained with 14 μg/ml acridine orange and 14 μg/ml ethidium bromide according to the protocol described in [25]. Briefly, after trypsinization, cells were collected by centrifugation (5 min, 300 × *g*), washed once and resuspended in a modified Krebs buffer containing both dyes. After 5-min incubation at room temperature in the dark, 10 μl of cell suspension was deposited on a microscope slide to examine nuclear morphology using a Zeiss Axiovert 40 CFL inverted microscope with SPOT RT-SE™ digital camera (Diagnostic Instruments Inc., MI, USA) using 20× objective lens. A total of 300 cells were accounted to determine cell viability and stages of apoptosis development.

Statistical analysis

Statistical analyses were performed with GraphPad Prism version 5.03 for Windows (GraphPad Software Inc., CA, USA). Results are expressed as mean ± SEM from at least three independent experiments. Statistically significant differences between MNP-loaded and unloaded samples were estimated by unpaired, two-tailed Student's *t*-test. Differences were considered significant at $p < 0.05$.

Results

The loading of primary rat endothelial cells with MNPs at the amount of 25.3 ± 0.75 pg magnetite/cell on a magnetic separator results in a similar loading pattern as was observed in bovine aortic endothelial cells shown in our earlier work [19]. After 24 h of incubation, the MNPs occupy intracellular space mostly perinuclearly. The resulting structural rearrangements of intracellular organelles could alter the functional state of cellular life-supporting systems. In this work, we studied the major intracellular infrastructures in order to evaluate the effects of internalized MNPs on cell structural and metabolic integrity and their potential for further proliferation.

Impact of MNP loading on cytoskeleton integrity

The cytoskeletal network is a biosensor of cellular well-being. It is ultimately involved in transport and localization of organelles. The microtubules and actin stress filaments were visualized by cell transfection with GFP-tubulin and EYFP-β-actin, respectively (Figure 1). Continuous actin (Figure 1A–E) and microtubules (Figure 1F–H) networks remain preserved, while MNPs locally displace actin (Figure 1B & D) and microtubules (Figure 1G) fibers rather than tear them apart. The thick arcs, dorsal and ventral actin fibers are not affected by internalized MNPs (Figure 1B & C).

Evaluation of the integrity of ER & its calcium capacity in MNP-loaded RAECs

ER has been visualized using ER-Tracker Blue-White DPX dye. Figure 2 demonstrates MNP-loaded (Figure 2A–C) and unloaded (Figure 2D & E) RAECs. For contrast microscopy in this experiment, we used fluorescent (red) MNPs. In the DIC image Figure 2A, MNPs in cytosole are seen as dark gray aggregates localized mostly around the nucleus. Although MNPs seem to co-occupy almost entire volume in the focal plane, cells preserve their original flat morphology. Arrows on Figure 2B & C indicate areas in the cellular interior where ER is displaced by MNP aggregates. We assumed that very locally ER cisterns could also be partially destroyed. This was confirmed by quantification of the amount of calcium released from the ER upon stimulation with thapsigargin.

In another experiment, RAECs preloaded with non-fluorescent MNPs and free calcium ions sensitive dye Fluo-4AM, were stimulated with 1 μM thapsigargin, which blocks Ca^{2+}-ATPase of the ER leading to release of free calcium ions into cytosole. To evaluate ER calcium capacity, calcium efflux from the extracellular environment was excluded by incubation of cells in Ca^{2+}-free buffer. The buffer was additionally supplied with 1 mM Ca^{2+} chelator EGTA. To avoid uptake of calcium released from the ER into mitochondria through mitochondria ATP-dependent Ca^{2+} uniporter, cells were pretreated with 2 μg/ml oligomycin. This inhibitor arrests mitochondria ATP-synthase preventing generation of energy necessary for Ca^{2+} transport. As seen in the Figure 2F, upon stimulation with thapsigargin, unloaded RAECs release to cytosole up to 388 ± 52.4 nmol calcium, while stimulation of MNP-loaded cells results in elevation of cytosolic calcium to about 271 ± 20.7 nmol.

Effects of MNP loading on RAECs mitochondria network organization, content & mitochondria functional integrity

Visualization of mitochondria in fluorescent (570 nm emission) MNP-loaded RAECs was performed by staining the mitochondria with specific dye Mito-Tracker Green. Since MitoTracker Green is a mitochondria membrane potential insensitive probe, it enables evaluation of the total mass of mitochondria in cells regardless of their mitochondria membrane polarization. The MitoTracker Green intensity data have been collected from individual cells within a focal plane. About 100 cells in several focal planes were accounted for each experiment and analyzed using FV10-ASW 1.7 Olympus Software. Mitochondrial network of control unloaded RAECs is presented in Figure 3A. Figure 3B & C shows that mitochondria in MNP-loaded cells remain non-swollen and elongated, indicating the functionally active organelles. MNPs do not seem to tightly associate with the organelles (Figure 3C and inclusion). Also we do not exclude the possibility that some mitochondria could be degraded being mechanically stressed by the internalized nanoparticles, and therefore the total mass of mitochondria in MNP-loaded cells is anticipated to be lower than in control unloaded cells. In agreement with this assumption, the total amount of mitochondria calculated by the MitoTracker Green intensity per cell has been shown to be decreased in MNP-loaded versus unloaded RAECs (Figure 3D).

The critical characteristic of the functional mitochondria is the level of their inner membrane potential. Although energy driving force in mitochondria depends both on pH gradient and

membrane potential Δ_m, membrane potential is determinant for many transport processes and is an indicator of compromised membrane structure or ATP production. Figure 3E demonstrates that MNP-loaded cells contain a larger population of mitochondria with higher membrane potential than unloaded cells.

Sufficient level of membrane potential is an important parameter providing support for cellular energy needs. To further evaluate intactness of the energy generating system of MNP-loaded cells, we analyzed the respiratory and oxidative phosphorylation (OxPhos) machinery of RAECs mitochondria. The typical representative respirometric recordings are presented in Figure 4A & B. Cells were treated with oligomycin, an inhibitor of mitochondria ATP synthase causing a drop in respiratory rates, and following stepwise titration with FCCP to reach maximum stimulation of respiration. FCCP is an uncoupler, which stimulates oligomycin inhibited respiration through pumping the protons back to mitochondria matrix omitting the ATPase. Routine state corresponds to basal unperturbed respiration. Leak respiration indicates residual electron transport after blocking the ATPase with oligomycin. The electron transport system (ETS) is a determination for the maximal mitochondria electron transport capacity. Figure 4C & D demonstrate the rates of oxygen consumption in MNP-loaded and unloaded RAECs at the described above respiratory conditions 24 and 48 h after loading with nanoparticles. It is evident that MNP-loading does not compromise the energetic system of mitochondria since the rates of oxygen flux in loaded and unloaded cells are very similar. The slightly higher value of the uncoupled respiration in MNP-loaded cells has been shown to be statistically insignificant. Overall, OxPhos activity did not change 48 h postincubation with MNPs, which demonstrates that MNPs do not alter the metabolic control system of cells, neither by their amount in cytosole nor by their chemical composition.

Evaluation of apoptosis induction probability

Upon loading, MNPs tend to occupy mainly a perinuclear area. This potentially could lead to rearrangement of cell ultrastructure and affect cell proliferation. To ensure that loading does not evoke cell death at later stages after loading, we assessed the induction of apoptotic and/or necrotic cell death in MNP-loaded RAECs 24 and 48 h postloading. Figure 5A shows that 86.37% of MNP-loaded cells are alive while only 13.3% of the population accounts the necrotic cells. Importantly, there is no increase in the amount of cells undergoing early apoptosis. The 0.33% is within the same normal range obtained for the unloaded, control cells (0.66%).

To further analyze the proliferative potential of MNP-loaded RAECs, cells were stained with acridine orange, an agent which specifically binds to the nucleic acids. Several MNP-loaded cells are demonstrated on DIC (Figure 5B) and confocal fluorescence (Figure 5C) images. Arrows indicate two cells densely packed with MNPs. Despite high MNP loading, the condensed chromatin in those cells more likely depicts a prometaphase of cell division cycle (Figure 5C).

Evaluation of IP_3 receptor-mediated calcium signaling as a mean of functional activity of MNP-loaded cells

Massive loading of cells with MNPs could cause significant structural reorganization of plasma membrane and alter its functional properties. We evaluated the functional stability of widely expressed PX2/PY2 purinergic membrane receptors [26] through analysis of their response upon stimulation with their ligand ATP [27]. Cells seeded on glass-bottom dishes and loaded with calcium sensitive dye Fluo-4AM were visualized at 60× magnification under the confocal microscope. The ATP was added by pipetting directly onto the cell culture dish. To confirm that calcium transients are not a result of flow-related mechanosensitization, a pure buffer was added to the cells in a dish by pipetting from above and gentle mixing. Liquid waves caused by addition of the buffer solution induced no calcium oscillations in the cytosole. In turn, 300 nM ATP provoked elevation of the intracellular calcium level (Figure 6). It should be noticed that higher ATP concentrations (10–50 μM) did not enhance the amplitude of Ca^{2+} spikes significantly. In RAECs, 300 nM ATP induces a rapid, transient increase in cytosolic calcium concentration, followed by irregular calcium oscillations (Figure 6B). The initial highly pronounced calcium spikes have been accounted for by comparison with effects of ATP addition on IP_3-dependent calcium transients in cytosole (Figure 6A). Confocal microscopy enables studying a limited number of cells per time interval. Therefore the variation of the microfluorimetry results is larger than in multi-million cell scale measurements. Each experimental focal plane encompassed 30–40 individual cells. The same pattern of the initial rapid calcium increase and propagating small calcium waves was observed after the second and third repetitive stimulations with the same dose of ATP. Despite similar calcium responses on nucleotide admin istration by both magnetically loaded and unloaded cells, the amplitude of calcium elevation was up to 239% higher in MNP-loaded cells than in unloaded cells (Figure 6A). This comparative data indicate that the purinergic receptors in magnetically loaded cells remain functionally intact although the entire calcium regulating system of RAECs becomes sensitized to the stimulation of the receptors upon loading with MNPs.

Discussion

MNPs find diverse biomedical applications due to their attractive chemical and physical properties. However, successful use of these systems with biological cells and tissues *in vivo* requires these systems to be biocompatible and nontoxic on various levels. In this work, we studied the impact of MNPs incorporated within the cytosole on the integrity of organelles infrastructure and their functional activity in primary endothelial cells isolated from rat aorta (RAEC). In contrast to transformed cell lines, primary cells are more relevant biological systems for investigation of the effects of internalized materials (polymeric MNPs in our study) on cellular well-being. RAECs are selected as a cell type that is currently being investigated by our group in magnetic stent targeting strategy for prevention of in-stent restenosis in rat model [3]. Successful therapeutic outcomes can be expected if delivered MNP-loaded cells efficiently adhere at the target site and metabolically adapt to a new environment, preserving their long-term functional activity and genetic stability. Importantly, both structural and functional intactness of MNP-loaded cells are crucial in

providing the therapeutic effect avoiding future undesired life threatening implications which could be caused by delivered cells.

The efficacy of cell loading with MNPs depends on the amount of particles added to cells and duration that cells and particles are exposed to a magnetic field. The dense loading of cells with MNPs (~25 pg magnetite/cell) can be achieved by incubation of ~300,000–350,000 primary endothelial cells with 0.0736 mg of polymer-based MNPs (a given dose of ~100 pg magnetite/cell for 48% w/w MNPs) for 24 h [19]. We focused on the short-term effects of the 25 pg magnetite/cell because this dose makes cells sufficiently responsive for magnetic targeting. The long-term effects of the MNPs on cells do not seem to be critical because with each cell division, the MNP content within daughter cells will logarithmically decrease, thus minimizing potential adverse effects. Internalization of MNPs within cells is a physical intervention that could interfere with the mechanosensing system of cells, including cytoskeletal complex. Actin and microtubules filaments attached to the membrane serve as mechanical sensors transmitting the mechanical stimulation further to biochemical responses. Cytoskeleton elements are involved in intracellular localization and trafficking of organelles and provide intracellular functional communication. For example, mitochondria movement is mainly associated with microtubules [28,29], however there is also a close relationship between mitochondria dynamics and their integration with actin filaments [30]. Therefore, the integrity of cytoskeleton filaments guarantees the metabolic stability of cell central energy supplying system. To determine the effect of magnetic particles on cellular skeletal dynamics, cells transfected with EYFP β-actin and GFP-tubulin were examined microscopically. We demonstrated that both actin and microtubule networks (Figure 1) are overall preserved, although locally, MNPs push the skeleton filaments displacing the cellular content rather than rupturing the cytoskeleton. This is also true for reticulated organelles, such as ER and mitochondria. As seen from Figures 2 & 3, ER and mitochondrial systems are significantly displaced by internalized MNPs. However, a detailed evaluation of the organelle content revealed that mitochondria and ER networks are partially degraded in places of MNPs massive accumulation with no apparent effects on overall cellular functions. It was important to evaluate the state of ER since its injury could result in reduced functionality or prolonged activation provoking generation of misfolded proteins and by that induce ER-stress pathway leading to cell pathology and subsequent tissue dysfunction. To understand this point, we evaluated ER stress imposed by MNPs utilizing ER stress agent, thapsigargin, which blocks ER Ca^{2+}-ATPase resulting in calcium release to cytosole [31]. Figure 2F demonstrates that a decreased amount of ER cisterns resulted in dropping the total amount of calcium released to cytosole after addition of thapsigargin. Importantly, decrease in MNP-loaded RAECs ER calcium content by 30% compared with unloaded cells did not alter overall calcium homeostasis and overall cellular activity as evidenced by preserved cellular metabolic and proliferative activity over 48 h after loading cells with MNPs. A similar decrease in the total organelle content was observed for the mitochondria network. The total mitochondria content was quantified by measuring the intensity of MitoTracker Green, a dye that incorporates into all cellular mitochondria regardless of their membrane potential level. Figure 3D shows that the total amount of mitochondria is decreased in MNP-loaded RAECs. Interestingly, although MNP-loaded cells lose part of their mitochondria pool, the remaining organelles demonstrate high membrane potential. At this condition, the

elevated membrane potential (Figure 3E) appears to be a cellular response to compensate for decreased number of mitochondria in MNP-loaded cells (Figure 3D) and enables the remaining mitochondria to acquire high energy efficiency to support metabolic needs of MNP-loaded cells.

It is of note, mitochondria do not tend to tightly associate with nanoparticles. The single focal plane shown in the inclusion to the Figure 3C depicts the spatial relationship between MNPs (red) and mitochondria (green) in the same cell. The loose association between MNPs and mitochondria prevents mechanical damage of mitochondria membrane by nanoparticles. In addition, mitochondria in MNP-loaded cells remain not swollen and well reticulated, which is an indication on their functional intactness. As the stability of mitochondria energy metabolism is central to meet energy demands of cell proliferation and other signaling and metabolic activities, we further evaluated mitochondria bioenergetic capacity that characterizes state of cell aerobic energy production [24]. High-resolution respirometry and inhibitor-protonophore titration protocols were applied to study oxidative phosphorylation of RAEC's mitochondria with and without MNP loading. To evaluate the oxygen consumption based solely on cell endogenous resources we conducted measurements in a buffer that does not contain respiratory substrates. The inhibitor-protonophore protocol enables to evaluate the activity of ATP synthase and integrity of mitochondria inner membrane. Routine respiration corresponds to unstimulated basal respiratory activity of cells. Uncoupled leak respiration is obtained in the presence of oligomycin, an agent specifically inhibiting the mitochondrial ATP synthesizing enzyme, so that no ATP can be produced. In the presence of oligomycin, the electron flow reflects the energy requirement to compensate for the proton leak. We observed that presence of MNPs within cells does not affect coupling of respiration and oxidative phosphorylation, as the respiratory rate after addition of oligomycin remains about 6 pmol O_2/s/10^6 cells in 24 and 48 h post MNP loading similar to the values in unloaded cells (Figure 4C & D). The maximum uncoupled respiratory activity measured in the presence of optimum protonophore concentration provides a measure of the maximum kinetic capacity of the mitochondria (ETS) and at given experimental condition provides an estimate of intrinsic uncoupling and therefore inner membrane integrity. Our data shows that in MNP-loaded RAECs the ETS values are not noticeably different from those in control cells. The maximum rates of oxygen consumption in the presence of FCCP, which uncouples mitochondria OxPhos resulting in collapse of membrane potential, 24 h after loading were 39.7 ± 3.5 pmolO_2/s/10^6cells in loaded cells versus 42.8 ± 2.8 pmolO_2/s/10^6cells in unloaded cells (Figure 4C & D) and these values were statistically non-significant. Similar results as of 37.2 ± 8.1 pmolO_2/s/10^6cells in unloaded cells versus 42.2 ± 1.2 pmolO_2/s/10^6cells in MNP-loaded cells were obtained 48 h after loading. The addition of antimycin, an inhibitor of respiratory complex III, and therefore the blocker of the respiratory system on one of its final gains, enables the estimation of the contribution of nonmitochondrial enzymatic oxygen utilization to the overall cellular oxygen consumption (residual oxygen consumption). We did not observe any differences in residual oxygen consumption parameters in both loaded and unloaded RAECs. Importantly, either at 24 or 48 h post-MNP loading, the resulting oxidative phosphorylation properties of MNP-loaded RAECs remained unaltered, being fully capable of supporting energy demands of cells loaded with MNPs, including their proliferative activities.

Nondisturbed proliferation of RAECs has been demonstrated at 24 h post loading in spite of very dense packing of cells with MNPs in the perinuclear zone (Figure 5). Elucidation of probability of apoptosis/necrosis induction as a result of mechanical perturbations caused by MNPs has been performed using acridine orange/ethidium bromide double staining assay. We did not observe typical signs of apoptosis evidenced by chromatin condensation, nuclear deformation and cell splitting on apoptotic bodies. However, the population of MNP-loaded cells displayed a larger fraction of necrotic cells versus control, unloaded cells. Although, a statistically significant higher number of necrotic cells 13.3 ± 5.5% was observed in MNP-loaded RAECs versus 3.98 ± 1.1% in control cells, the remaining 86.37% of MNP-loaded cells were capable to recover the entire cell population as evidenced by their active proliferation.

To gain insights on possible MNP-provoked cell metabolic modulations, we also evaluated inositol triphosphate-dependent calcium signaling mediated by G-protein-associated plasma membrane purinergic receptors. It is known that P2 receptors mediate regulation of endothelial cells by extracellular nucleotides (adenosine triphosphate, adenosine diphosphate, uridine triphosphate and uridine diphosphate), including maintaining vascular tone, release of endothelial factors, such as prostaglandins, nitric oxide, endothelium-derived hyperpolarizing factor, agglutination of platelets and others [32–35]. The mechanical stress across the plasma membrane of endothelial cells caused by MNPs penetration can directly activate receptors, if not to cause their irreversible damage [36].

Administration of 300 nM ATP to unloaded RAECs resulted in a spike-like increase in cytosolic calcium, which was fully recovered to the initial level in a few seconds. MNP-loaded cells maintained similar calcium response but of a higher amplitude. This type of response is different from that of nonendothelial cells, which typically produce cytosolic calcium oscillations after addition of the below-threshold concentration of ATP. Such one-time oscillatory response usually cannot be obtained by further administration of ATP in a short period of time. In contrast, RAECs are capable of responding to the repetitive additions of 300 nM doses of ATP in short intervals by gradually decreasing calcium spikes. Overall ATP-induced calcium response of MNP-loaded RAECs has been shown to be higher versus unloaded cells, indicating that MNPs penetration and accumulation in cytosole could sensitize IP_3-dependent calcium processes by yet unknown mechanisms. Importantly, the resting cytosolic calcium level in MNP-loaded cells was not elevated, which is a sign of unperturbed calcium homeostasis. All together these facts indicate that presence of MNPs does not promote activation of calcium-mediated processes and therefore does not disturb normal cell homeostasis. However, higher calcium response in MNP-loaded RAECs to ATP stimulus could be a consequence of modulated by nanoparticles cytoskeleton organization (Figure 1) and cytoskeleton association with plasma membrane constituents, including purinergic and other receptors, which in turn sensitizes the receptors to the external factors.

Conclusion

In conclusion, loading RAECs with MNPs sets in motion some changes in cell metabolic homeostasis necessary to support cell functionality under stressful conditions caused by MNPs internalization. This comprehensive study of both structural features and metabolic

functions of cells demonstrated that studied polymer-based MNPs of given chemical composition, size, surface charge and dose do not induce significant adverse effects on cellular integrity. Our results are specific to the MNP type used in this study and could not be directly extrapolated to other types of magnetic particles. Moreover, loaded primary endothelial cells are capable of maintaining their normal rate of proliferation, calcium signaling and mitochondria energy metabolism, which are the key factors of cellular well-being. Finally, this study provides supportive evidence of safe applicability of MNP-loaded primary endothelial cells in potential cell therapy applications.

Future perspective

In the development of future clinical implementations for magnetic cell therapy, it is imperative that no adverse effects are caused by the introduction of nanomagnetic materials to the delivered cells or to the patient. Many previous studies have determined these effects to be minimal at therapeutic concentrations. Examples include the effect of MNP on organ toxicity in mice and rats through histological analyses [37,38], viability of human umbilical vein endothelial cells upon addition of the MNPs in a colorimetric MTT assay [39], and viability and proliferation of human endothelial cell line ECV-304 [40]. However, demonstrating that the loading of cells with MNP causes neither system nor cytotoxicity is not sufficient to ensure that the intended therapeutic efficacy of the cells is obtained. In addition, it is necessary to verify that the MNP loading causes no adverse effects to the functionality of major cell organelles. This is essential to guarantee metabolic stability of the central energy supplying system, the cell trafficking machinery and the signaling and proliferative apparatus of the cell which collectively ensures proper cell activity and lifespan necessary for achieving a desired therapeutic goal. In this study, we examined in detail the effects of internalized polymeric MNPs on cell structural and metabolic integrity and cell potential for further proliferation. Intactness of cytoskeleton elements and major organelles, such as ER and mitochondria, involved in cellular calcium and energy homeostasis, were investigated to validate magnetically loaded cells functional competence and stability.

As researchers develop the ever-expanding field of nanocarriers for delivery of drugs, genes and cells, there is a growing need to systematically assess effects of these nano-scale systems on biological activity and toxicity on various levels. Nanocarriers may interfere with some functions of proteins on the surface of cells, or cause toxicological effects on the level of nucleic acids, intracellular organelles, cytoskeleton or function of intracellular molecules once internalized inside cells. As of today, there is no agreed international standard on the toxicology and biocompatibility of nanocarriers. Thus, while these systems are in development, clinical trials or clinical use, further research and development of standards on their biocompatibility must be extended to enable safe use of such nano-scale systems in therapeutic applications.

Acknowledgments

The authors greatly appreciate assistance of Lee D Silver from Anatomy and Cell Biology Shriners Hospitals Pediatric Research Center at Temple University (PA, USA) in generating EYFP β-actin plasmid and in cell transfection experiments. We also thank Peter Baas and Shen Lin at Drexel University, College of Medicine (PA, USA) for providing us with GFP-tubulin plasmid. We thank Mikhail Medved from the Department of Surgery at Drexel University, College of Medicine (PA, USA) for the technical assistance.

References

Papers of special note have been highlighted as: • of interest;

•• of considerable interest

1. Alexiou C, Arnold W, Klein RJ, et al. Locoregional cancer treatment with magnetic drug targeting. Cancer Res. 2000; 60(23):6641–6648. [PubMed: 11118047]
2. Polyak B, Friedman G. Magnetic targeting for site-specific drug delivery: applications and clinical potential. Expert Opin Drug Deliv. 2009; 6(1):53–70. [PubMed: 19236208]
3••. Polyak B, Fishbein I, Chorny M, et al. High field gradient targeting of magnetic nanoparticle-loaded endothelial cells to the surfaces of steel stents. Proc Natl Acad Sci USA. 2008; 105(2): 698–703. High-quality study demonstrating the feasibility of magnetically mediated endothelial cell targeting to magnetizable intravascular stents *in vitro* and *in vivo*. [PubMed: 18182491]
4. Werner N, Junk S, Laufs U, et al. Intravenous transfusion of endothelial progenitor cells reduces neointima formation after vascular injury. Circ Res. 2003; 93(2):e17–e24. [PubMed: 12829619]
5•. Patel SD, Waltham M, Wadoodi A, Burnand KG, Smith A. The role of endothelial cells and their progenitors in intimal hyperplasia. Ther Adv Cardiovasc Dis. 2010; 4(2):129–141. A good review on mechanism of intimal hyperplasia highlighting the important attenuating role played by a functional endothelium. [PubMed: 20200200]
6. Casscells W. Migration of smooth muscle and endothelial cells. Critical events in restenosis. Circulation. 1992; 86(3):723–729. [PubMed: 1516183]
7••. Douglas G, Van Kampen E, Hale AB, et al. Endothelial cell repopulation after stenting determines in-stent neointima formation: effects of bare-metal vs. drug-eluting stents and genetic endothelial cell modification. Eur Heart J. 2013; 34(43):3378–3388. Very sound work showing that targeting endothelial cell function is a rational therapeutic strategy to improve vascular healing and decrease neointima formation after stenting. [PubMed: 23008511]
8••. Kipshidze N, Dangas G, Tsapenko M, et al. Role of the endothelium in modulating neointimal formation: vasculoprotective approaches to attenuate restenosis after percutaneous coronary interventions. J Am Coll Cardiol. 2004; 44(4):733–739. Considering endothelial denudation as one of the most important mechanisms contributing to restenosis, the authors focus more attention on methods of accelerating restoration of endothelial continuity. [PubMed: 15312851]
9. Larsen K, Cheng C, Tempel D, et al. Capture of circulatory endothelial progenitor cells and accelerated re-endothelialization of a bio-engineered stent in human *ex vivo* shunt and rabbit denudation model. Eur Heart J. 2012; 33(1):120–128. [PubMed: 21733913]
10. Schwartz RS, Holmes DR Jr, Topol EJ. The restenosis paradigm revisited: an alternative proposal for cellular mechanisms. J Am Coll Cardiol. 1992; 20(5):1284–1293. [PubMed: 1401633]
11. Asahara T, Chen D, Tsurumi Y, et al. Accelerated reconstitution of endothelial integrity and endothelium-dependent function after *phVEGF165* gene transfer. Circulation. 1996; 94(12):3291–3302. [PubMed: 8989143]
12. Hedman M, Hartikainen J, Syvanne M, et al. Safety and feasibility of catheter-based local intracoronary vascular endothelial growth factor gene transfer in the prevention of postangioplasty and in-stent restenosis and in the treatment of chronic myocardial ischemia: Phase II results of the Kuopio Angiogenesis Trial (KAT). Circulation. 2003; 107(21):2677–2683. [PubMed: 12742981]
13. Losordo DW, Isner JM, Diaz-Sandoval LJ. Endothelial recovery: the next target in restenosis prevention. Circulation. 2003; 107(21):2635–2637. [PubMed: 12782613]
14. Fatema Z, Medved M, Lazareva N, Polyak B. Functional behavior and gene expression profile of primary endothelial cells loaded with polymeric magnetic nanoparticles for targeted delivery to vascular stents. Nanomedicine (London). 2015; 10(9):1391–1406.
15. Macdonald C, Friedman G, Alamia J, Barbee K, Polyak B. Time-varied magnetic field enhances transport of magnetic nanoparticles in viscous gel. Nanomedicine (London). 2010; 5(1):65–76.
16. Johnson B, Toland B, Chokshi R, Mochalin V, Koutzaki S, Polyak B. Magnetically responsive paclitaxel-loaded biodegradable nanoparticles for treatment of vascular disease: preparation, characterization and *in vitro* evaluation of anti-proliferative potential. Curr Drug Deliv. 2010; 7(4): 263–273. [PubMed: 20695837]

17. Tengood JE, Alferiev IS, Zhang K, Fishbein I, Levy RJ, Chorny M. Real-time analysis of composite magnetic nanoparticle disassembly in vascular cells and biomimetic media. Proc Natl Acad Sci USA. 2014; 111(11):4245–4250. [PubMed: 24591603]

18•. Adams CF, Rai A, Sneddon G, Yiu HH, Polyak B, Chari DM. Increasing magnetite contents of polymeric magnetic particles dramatically improves labeling of neural stem cell transplant populations. Nanomedicine. 2015; 11(1):19–29. An interesting study describing a strategy to improve magnetic nanoparticle loading in hard-to-load neural stem cell population. [PubMed: 25038496]

19•. Macdonald C, Barbee K, Polyak B. Force dependent internalization of magnetic nanoparticles results in highly loaded endothelial cells for use as potential therapy delivery vectors. Pharm Res. 2012; 29(5):1270–1281. Demonstrates that endothelial cell uptake of MNPs is a force dependent process which highly depends on reorganization of cell cytoskeleton. [PubMed: 22234617]

20. Macdonald C, Friedman G, Alamia J, Barbee K, Polyak B. Time-varied magnetic field enhances transport of magnetic nanoparticles in viscous gel. Nanomedicine. 2010; 5(1):1–12. [PubMed: 20025457]

21. Grynkiewicz G, Poenie M, Tsien RY. A new generation of Ca^{2+} indicators with greatly improved fluorescence properties. J Biol Chem. 1985; 260(6):3440–3450. [PubMed: 3838314]

22. Gnaiger E, Steinlechner-Maran R, Mendez G, Eberl T, Margreiter R. Control of mitochondrial and cellular respiration by oxygen. J Bioenerg Biomembr. 1995; 27(6):583–596. [PubMed: 8746845]

23. Pesta D, Gnaiger E. High-resolution respirometry: OXPHOS protocols for human cells and permeabilized fibers from small biopsies of human muscle. Methods Mol Biol. 2012; 810:25–58. [PubMed: 22057559]

24. Gnaiger, E. Polarographic oxygen sensors, the oxygraph and high-resolution respirometry to assess mitochondrial function. In: Dykens, JA.; Will, Y., editors. Mitochondrial Dysfunction In Drug-Induced Toxicity. Wiley; 2008. p. 27-352.

25. Kasibhatla S, Amarante-Mendes GP, Finucane D, Brunner T, Bossy-Wetzel E, Green DR. Acridine orange/ethidium bromide (AO/EB) staining to detect apoptosis. CSH Protoc. 2006; 2006(3) (Epub ahead of print). 10.1101/pdb00.prot4493

26. Abbracchio MP, Burnstock G, Boeynaems JM, et al. International Union of Pharmacology LVIII: update on the P2Y G protein-coupled nucleotide receptors: from molecular mechanisms and pathophysiology to therapy. Pharmacol Rev. 2006; 58(3):281–341. [PubMed: 16968944]

27. O'Connor SE, Dainty IA, Leff P. Further subclassification of ATP receptors based on agonist studies. Trends Pharmacological Sci. 1991; 12(4):137–141.

28. Heggeness MH, Simon M, Singer SJ. Association of mitochondria with microtubules in cultured cells. Proc Natl Acad Sci USA. 1978; 75(8):3863–3866. [PubMed: 80800]

29. Bernier-Valentin F, Aunis D, Rousset B. Evidence for tubulin-binding sites on cellular membranes: plasma membranes, mitochondrial membranes, and secretory granule membranes. J Cell Biol. 1983; 97(1):209–216. [PubMed: 6863392]

30. De Vos KJ, Allan VJ, Grierson AJ, Sheetz MP. Mitochondrial function and actin regulate dynamin-related protein 1-dependent mitochondrial fission. Curr Biol. 2005; 15(7):678–683. [PubMed: 15823542]

31. Thastrup O, Cullen PJ, Drobak BK, Hanley MR, Dawson AP. Thapsigargin, a tumor promoter, discharges intracellular Ca^{2+} stores by specific inhibition of the endoplasmic reticulum $Ca^{2(+)}$-ATPase. Proc Natl Acad Sci USA. 1990; 87(7):2466–2470. [PubMed: 2138778]

32. Bauer V, Sotnikova R. Nitric oxide–the endothelium-derived relaxing factor and its role in endothelial functions. Gen Physiol Biophys. 2010; 29(4):319–340. [PubMed: 21156995]

33. Communi D, Janssens R, Suarez-Huerta N, Robaye B, Boeynaems JM. Advances in signalling by extracellular nucleotides. The role and transduction mechanisms of P2Y receptors. Cell Signal. 2000; 12(6):351–360. [PubMed: 10889463]

34. Kunapuli SP, Daniel JL. P2 receptor subtypes in the cardiovascular system. Biochem J. 1998; 336(Pt 3):513–523. [PubMed: 9841859]

35. Wang L, Karlsson L, Moses S, et al. P2 receptor expression profiles in human vascular smooth muscle and endothelial cells. J Cardiovasc Pharmacol. 2002; 40(6):841–853. [PubMed: 12451317]

36. Chachisvilis M, Zhang YL, Frangos JA. G protein-coupled receptors sense fluid shear stress in endothelial cells. Proc Natl Acad Sci USA. 2006; 103(42):15463–15468. [PubMed: 17030791]

37•. Jain TK, Reddy MK, Morales MA, Leslie-Pelecky DL, Labhasetwar V. Biodistribution, clearance, and biocompatibility of iron oxide magnetic nanoparticles in rats. Mol Pharm. 2008; 5(2):316–327. Focuses on biodistribution, clearance and biocompatibility of magnetic nanoparticles for *in vivo* biomedical applications to ensure their safe clinical use. [PubMed: 18217714]

38. Kim JS, Yoon TJ, Yu KN, et al. Toxicity and tissue distribution of magnetic nanoparticles in mice. Toxicol Sci. 2006; 89(1):338–347. [PubMed: 16237191]

39•. Hafeli UO, Riffle JS, Harris-Shekhawat L, et al. Cell uptake and *in vitro* toxicity of magnetic nanoparticles suitable for drug delivery. Mol Pharm. 2009; 6(5):1417–1428. The authors focus on biocompatibility and toxicity of magnetic nanoparticles. [PubMed: 19445482]

40. Yang FY, Yu MX, Zhou Q, Chen WL, Gao P, Huang Z. Effects of iron oxide nanoparticle labeling on human endothelial cells. Cell Transplant. 2012; 21(9):1805–1820. [PubMed: 22776829]

Executive summary

The need to assess biocompatibility of magnetic nanoparticles

- To successfully translate magnetically mediated cell targeting from bench to bedside, there is a need to systematically assess the potential adverse effects of magnetic nanoparticles (MNPs) interacting with ‘therapeutic’ cells.

The impact of MNPs on cell structural integrity

- Polymeric MNPs displace cytoskeleton filaments locally in areas of their accumulation, however continuous actin and microtubules networks overall remain preserved.
- MNPs rearrange the endoplasmic reticulum (ER) resulting in decreased number of ER cisterns. However, decreased ER calcium content did not alter overall calcium homeostasis and overall cellular activity as evidenced by preserved cellular metabolic and proliferative activity over 48 h after loading cells with MNPs.

Effects of MNPs on mitochontria & cell metabolic activity

- Mitochondria displayed normal nonswollen and elongated morphology. Although the total number of mitochondria was reduced due to MNPs internalization, the remaining mitochondria acquire higher membrane potential enabling them to support cell energy demands.
- Rates of oxygen consumption in both MNP-loaded and unloaded cells were found to be comparable.

Effects of MNPs on induction of apoptosis & cell proliferation

- Typical signs of apoptosis evidenced by chromatin condensation, nuclear deformation and cell splitting on apoptotic bodies were not observed in both MNP-loaded and unloaded cells.
- MNP-loaded primary endothelial cells maintained their normal rate of proliferation, calcium signaling and mitochondria energy metabolism.

Conclusion

- This study provides supportive evidence that MNPs at doses necessary for targeting did not induce significant adverse effects on structural integrity and functionality of primary endothelial cells.

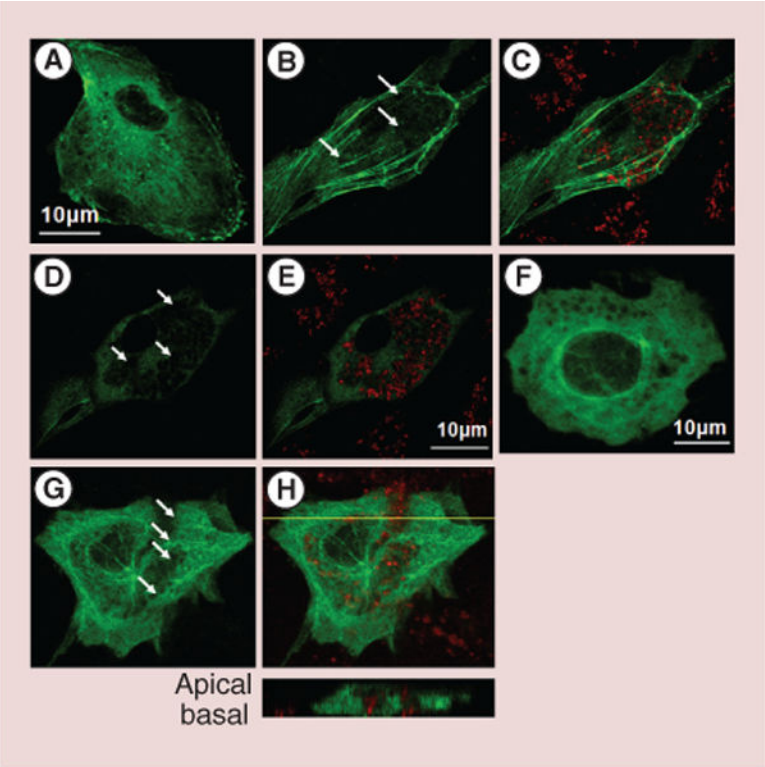

Figure 1. Rearrangement of cytoskeleton upon loading with magnetic nanoparticles

Primary rat aortic endothelial cells (RAECs) were transfected with green EYFP-β-actin and green GFP-tubulin for 24 h and loaded overnight with red BODIPY®564/570 nm magnetic nanoparticles (MNPs). The unloaded cell actin skeleton is presented on confocal image **(A).** The images **(B–E)** demonstrate two focal planes of a single cell expressing EYFP-β-actin: **(B & D)** actin skeleton, **(D & E)** merged images of the actin skeleton and MNPs. Arrows indicate the local actin network rearrangements. Although thicker fibers, such as arcs, dorsal and ventral stress filaments are not affected, the aggregated MNPs seem to displace thin fibers forming holes in continuous actin network. **(F–H)** Z-stack images of cells expressing fluorescent microtubules. **(F)** Demonstrates unloaded RAEC expressing GFP-tubulin. **(G)** GFP-tubulin expressing cell loaded with fluorescent MNPs (particles are not shown). **(H)** Merged image of microtubules network and MNPs. Arrows indicate local filament rearrangements. The inclusion is the vertical slice corresponding to the optical plane designated on the confocal image by the yellow line demonstrating localization of MNPs among microtubules.

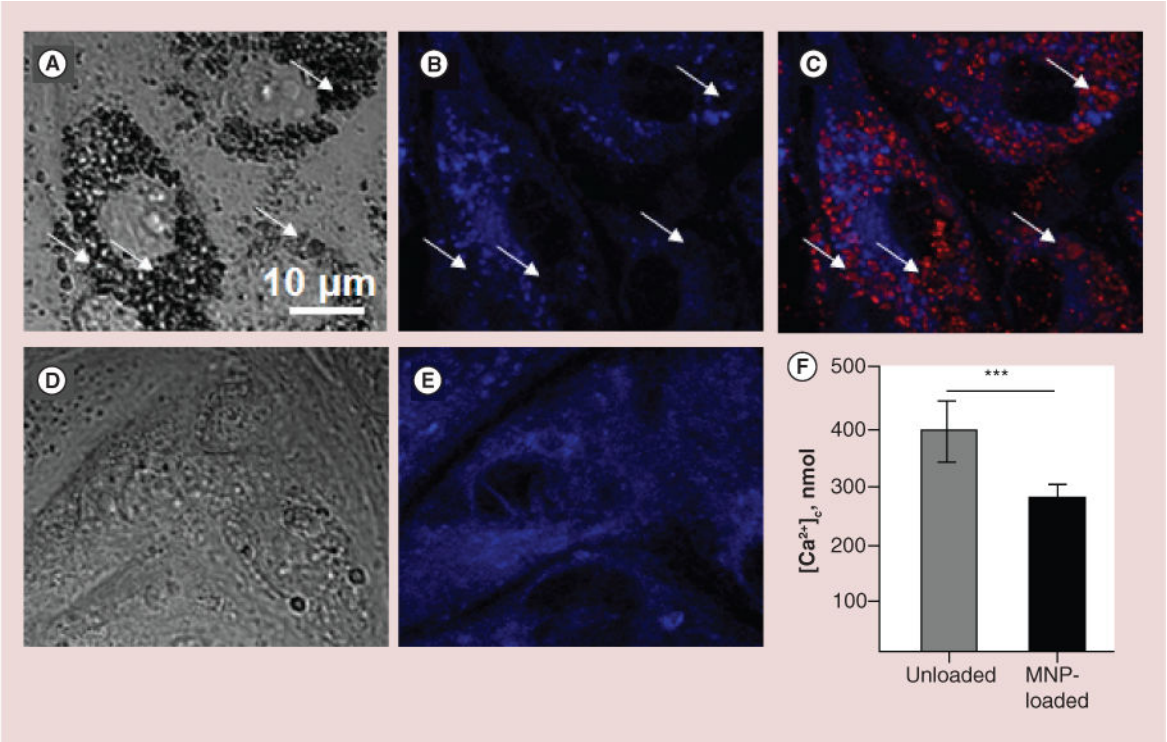

Figure 2. Characterization of structural rearrangement of endoplasmic reticulum and evaluation of its calcium capacity after cell loading with magnetic nanoparticles

First, cells were loaded for 24 h with BODIPY®564/570-MNPs and after that, ER was visualized using ER-Tracker Blue-White DPX as it is described in the 'Methods' section. It was observed that embedding of MNPs into cytosole rearranges ER network, which results in diminished calcium resource of ER. **(A–C)** Images of primary rat aortic endothelial cells (RAECs) loaded with MNPs. **(A)** DIC image demonstrates large amount of MNPs in cells seen as black aggregates. **(B & C)** Confocal images of ER only and merged image of MNPs (red) and ER (blue). Arrows indicate areas where ER was displaced by MNPs. **(D & E)** DIC and confocal images of MNP-unloaded RAECs. **(F)** To validate the effect of MPNs on the amount of free calcium in ER, the calcium release was provoked by 1 μM thapsigargin in Ca^{2+}-free buffer containing 1mM EGTA. To avoid leak of calcium released from ER into mitochondria, the mitochondrial calcium uptake was blocked by cell pretreatment with 2 μg/ml oligomycin, which prevents ATP-dependent Ca^{2+} uniport into mitochondria. Amplitude of cytosolic calcium peak as a result of ER stress was measured fluorimetrically on the confocal microscope. Data presented as mean ± SEM (n = 72 and 75 cells, accordingly), $p < 0.0001$.

MNP: Magnetic nanoparticle.

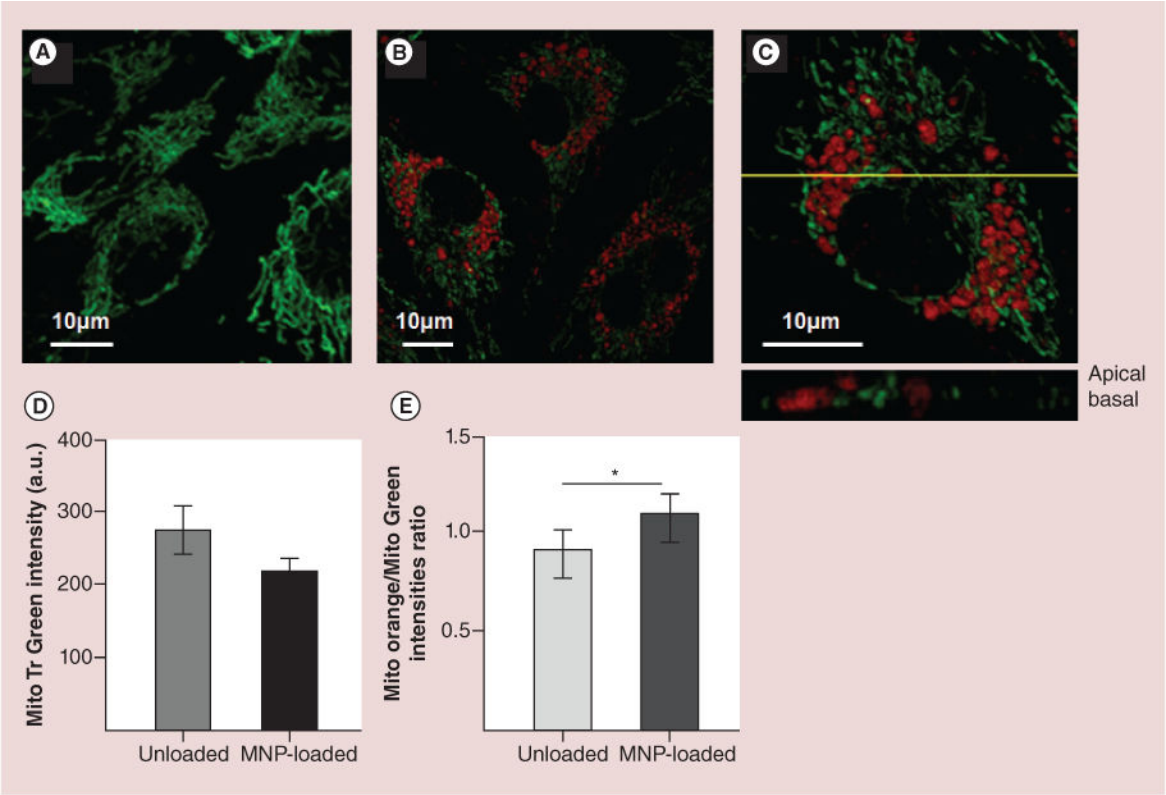

Figure 3. Confocal imaging and quantification of mitochondria mass and membrane potential in magnetic nanoparticles-loaded and unloaded primary rat aortic endothelial cells

Mitochondria were labeled with membrane-insensitive dye, MitoTracker Green (70nM). BODIPY®564/570 nm-MNPs were used to discern them from mitochondria. **(A)** Confocal image of mitochondria in unloaded primary rat aortic endothelial cells (RAECs). **(B)** The image of RAECs loaded with MNPs for 24 h. **(C)** Magnified image of a single cell presented in image B. The yellow line depicts the optical plane demonstrating localization of MNPs among mitochondria. It is clear that nanoparticles do not co-localize with organelles but rather deflect them. **(D)** Flow cytometry data of mitochondria mass quantified as a mean of MitoTracker Green intensity collected from unloaded and MNP-loaded RAECs. 10^4 cells were accounted in each experiment. Data presented as mean ± SEM (n = 3), statistically ns. **(E)** Comparative quantification of the distribution of mitochondria populations with high and low membrane potential in MNPs loaded and unloaded RAECs. Cell mitochondria were double labeled with membrane potential sensitive (MitoTracker Orange) and insensitive (MitoTracker Green) dyes and analyzed flow cytometrically. Data presented as mean ± SEM (n = 3), $p < 0.0001$.

MNP: Magnetic nanoparticle.

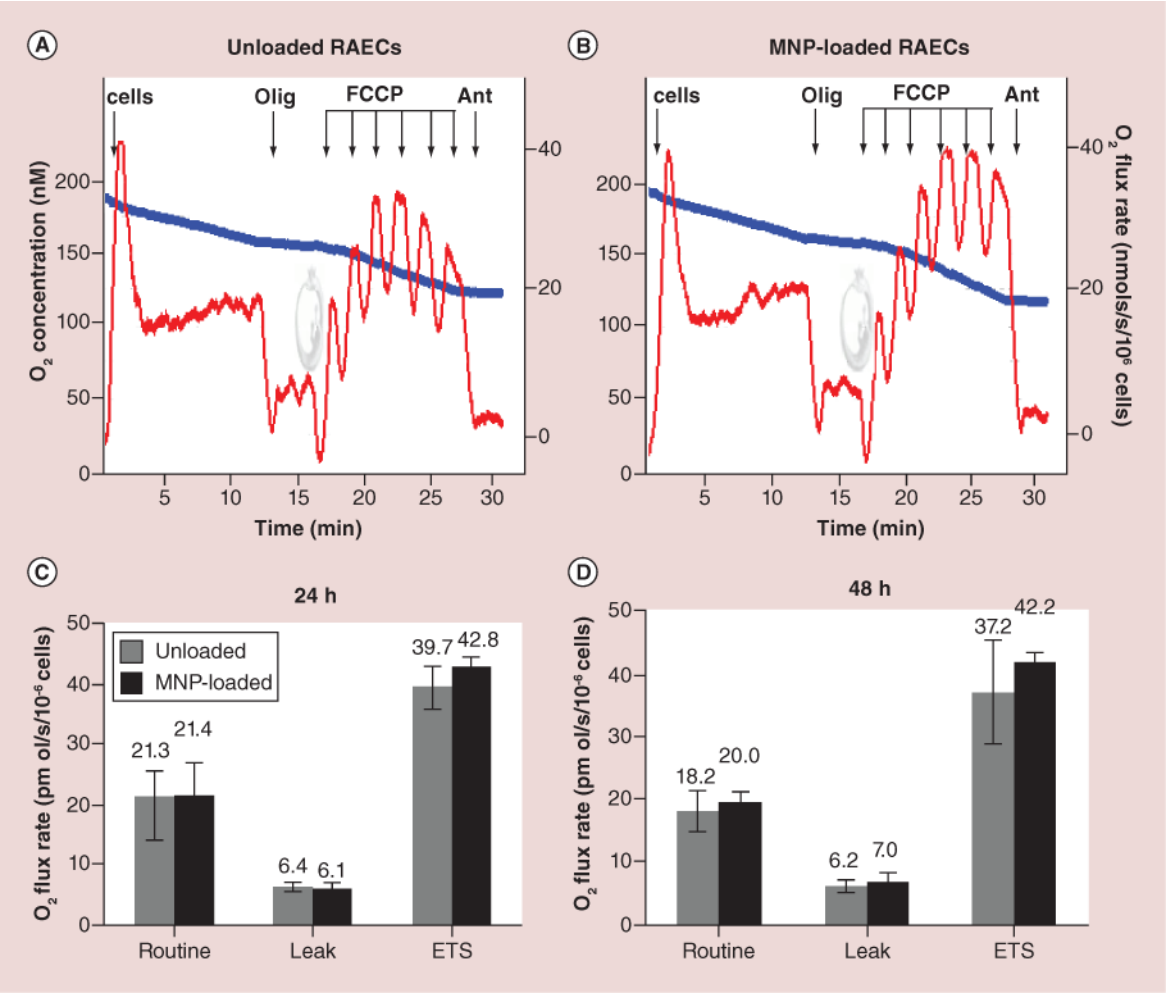

Figure 4. Respiration and oxidative phosphorylation in magnetic nanoparticles-loaded versus unloaded primary rat aortic endothelial cells

(A & B) The typical steady-state oxygen flux records at different states of uncoupled and stimulated respiration for unloaded and MNP-loaded RAECs. Blue traces are changes in O_2 concentration in the closed chamber as a result of oxygen consumption by cellular mitochondria. Red traces are rates of oxygen fluxes calculated using Oroboros DataLab software as the negative time derivative of O_2 concentration. **(C & D)** Respiration data were generated by stepwise analysis of respiratory system constituents at 24 and 48 h after cell loading with MNPs. Routine is a basal nonperturbed respiration. Leak by definition is O_2 flux compensating for proton leak measured after inhibition of ATPase with oligomycin. ETS refers to mitochondria maximal respiratory capacity. This maximally stimulated respiration state is induced by titration with low doses of uncoupler FCCP in order to reach the maximally stimulated respiration prior to inhibition of respiration occurs (decline of red traces upon FCCP addition). The addition of antimycin blocks mitochondria respiration. The residual respiration accounting for nonmitochondrial portion of oxygen utilization (residual oxygen consumption) was shown to be similar in both unloaded and loaded cells. Additions: 1×10^6 cell/ml, 2 μg/ml oligomycin, titration by 20 nM dose of FCCP, 2.5 μM antimycin.

The numbers above columns are rates of respiration expressed in pmol O_2/s/10^6 cells. Data presented as mean ± SEM (n = 3–4) and are shown to be statistically non-significant.
MNP: Magnetic nanoparticle; RAEC: Primary rat aortic endothelial cell.

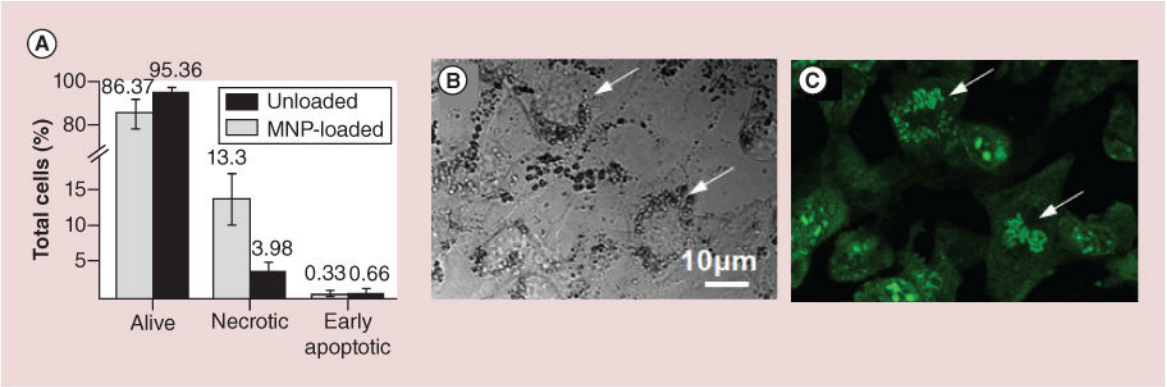

Figure 5. Evaluation of apoptosis in magnetic nanoparticles-loaded versus unloaded primary rat aortic endothelial cells and observation of cell proliferative activity

(A) The statistics of apoptosis induction was analyzed by microscopy using acridine orange/ethidium bromide double staining. The numbers above the columns are the percentage of cells at each indicated condition. **(B & C)** Primary rat aortic endothelial cells were loaded with nonfluorescent MNPs overnight and rinsed from nonincorporated particles. Just before imaging, cells were preincubated for 10 min with acridine orange which binds to the nucleic acids. Arrows indicate cells containing large amount of MNPs and undergoing active mitosis.

MNP: Magnetic nanoparticle.

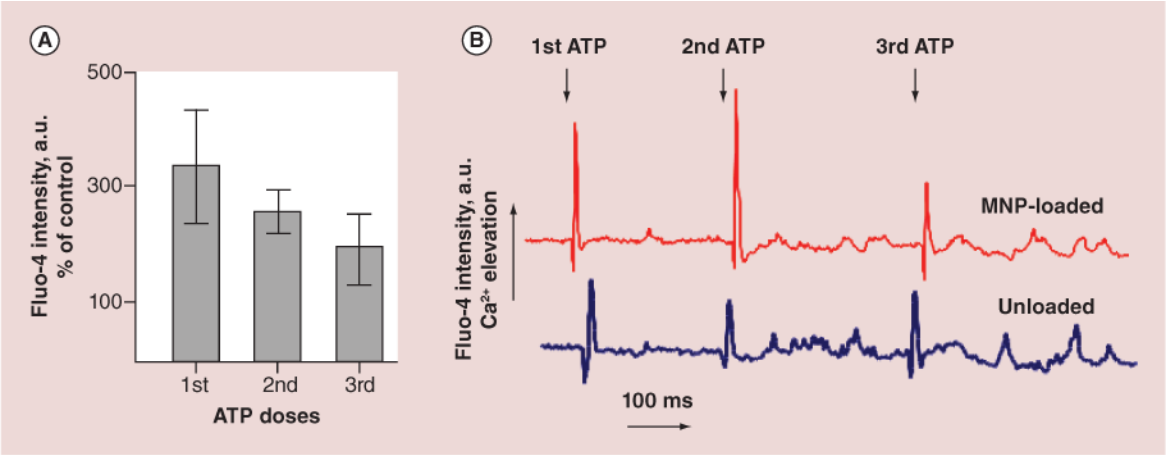

Figure 6. Calcium response evoked by three-phase administration of exogenous ATP to magnetic nanoparticles-loaded and unloaded primary rat aortic endothelial cells

Plasma membrane purinergic receptors-mediated cytosolic calcium elevation has been stimulated by addition of 300 nM ATP with about 200–300 ms interval to enable complete recovery of the signal to the basal level. **(A)** Data of cytosolic calcium changes were read as a fluorescence intensity of Fluo-4AM and presented as a percent of the fluorescence emission changes in magnetic nanoparticle-loaded versus unloaded cells (% of control: first ATP – 339%, second ATP – 259% and third ATP – 202%, correspondingly). **(B)** Representative records of cytosolic calcium transients upon ATP stimulation.